HIV-1 Membrane Fusion Mechanism: Structural Studies of the Interactions between Biologically-Active Peptides from gp41

Mary K. Lawless,* Shawn Barney, Kelly I. Guthrie, Teresa B. Bucy, Stephen R. Petteway, Jr.,‡ and Gene Merutka*

Trimeris, Inc., P.O. Box 13963, Research Triangle Park, North Carolina 27709

Received March 22, 1996⊗

ABSTRACT: Two synthetic peptides corresponding to sequences in HIV-1_{LAI} gp41, T21 (aa 558−595) and T20 (aa 643−678), are strong inhibitors of HIV-1 viral fusion, having EC_{50} values of 1 μg/mL and 1 ng/mL, respectively. Previous work suggested that T21 forms a coiled-coil structure in PBS solution, while T20 is primarily nonhelical, and that the inhibitory action of these peptides occurs after the interaction between the viral gp120 protein and the cellular CD4 receptor [Wild, C. T., Shugars, D. C., Greenwell, T. K., McDanal, C. B., Matthews, T. J. (1994) *Proc. Natl. Acad. Sci. U.S.A. 91,* 9770 and references therein]. The current study uses sedimentation equilibrium (SE), circular dichroism (CD), and viral-fusion assays to quantitatively investigate peptide structure and peptide−peptide interactions. SE analyses of T21 (1−100 μM) indicate that the peptide self-associates via a monomer/dimer/tetramer equilibrium; in addition, T20 is monomeric in the range of 1−10 μM and exhibits a complicated monomer/tetramer equilibrium between 20 and 100 μM. Singular value decomposition analyses of the CD spectra of T21 and T20 indicate that the helical content of these peptides in PBS solution is 90% and 20%, respectively. A structural interaction between the two peptides is detected by CD at several concentration ratios of T20:T21. These experiments emphasize that T20 interacts specifically with the tetrameric form of T21. Truncated forms of T20 also exhibit structural interactions with T21 at varying concentration ratios. The ability of T20 and the truncated peptides to interact structurally with tetrameric T21 correlates with antiviral activity. Implications of these findings are discussed in terms of proposed mechanisms of membrane fusion inhibition and the structural changes which occur in gp41 during membrane fusion.

Membrane attachment and fusion are the first steps in the cellular infection process by many enveloped viruses (Wiley & Skehel, 1990). The membrane fusion events leading to human immunodeficiency virus type 1 (HIV-1) infection are initiated by recognition of the T-cell host by HIV-1, occurring via binding of the outer surface viral glycoprotein gp120 to the T-cell receptor CD-4 (Dalgleish et al., 1984). The HIV-1 transmembrane fusion protein gp41, noncovalently associated with gp120, is exposed after this binding (Hart et al., 1991; Kirsh et al., 1990). Subsequent structural changes in gp41 (Sattentau & Moore, 1991) facilitate the insertion of the fusion peptide (located at the gp41 N-terminus) into the host cell membrane. This event is followed by fusion of the two membranes and mixing of the cellular and viral contents.

The best understood mechanism of viral fusion is that of the influenza virus (Bullough et al., 1994; Carr & Kim, 1993; Wilson et al., 1981). In this system, the fusion event is initiated by uptake of the virion into a cellular endosome, resulting in structural changes in the fusion protein hemagglutinin (HA) by the resulting low pH environment. HA consists of a trimer of dimers, and each dimer consists of a membrane-anchored segment (HA_2), forming the trimeric coiled-coil structure responsible for the oligomerization of the protein, and the HA_1 segment which covers this inner core. The low pH change induces the displacement of HA_1 from HA_2; this causes the B-loop region of HA_2 to spring into an extended coiled-coil structure, directing the hydrophobic fusion peptide sequence from its location inside the protein toward the target membrane.

Although the HIV-1 fusion process is pH independent, the comparison to influenza is potentially useful since several regions of the HIV-1 transmembrane protein gp41 have been shown to have high propensities to form coiled coils (Gallaher et al., 1989). Although much information has been gathered regarding HIV-1 induced membrane fusion, the structural and functional role of gp41 in this process has not been clearly defined. Data indicating structural changes within gp41 have recently been reviewed and two models of HIV fusion proposed (Matthews et al., 1994).

Two synthetic peptides T21 and T20 (designated DP107 and DP178 in the original publications), corresponding to sequences from gp41, have previously been shown to block virus-mediated cell-to-cell fusion and *de novo* HIV-1 infection of T-cells with 50% effective concentration values (EC_{50}) of 1 μg/mL and 0.001 μg/mL, respectively (Wild et al., 1992, 1994b). The regions of gp41 containing the sequences of both peptides were predicted to form coiled coils, yet only T21 has been shown to adopt significant helical structure in solution, while T20 was suggested to have a primarily random structure in solution (Gallaher et al., 1989; Wild et al., 1992, 1994b). Figure 1 illustrates the portions of gp41 from which these peptides were derived.

Previous experiments on the regions of gp41 corresponding to these peptides indicated that an interaction between these two discontinuous domains must exist in the native or

* Authors to whom correspondence should be addressed.

‡ Present address: Bayer Corp., Pharmaceutical Division, Biological Products, 8368 US 70 W., P.O. Box 507, Clayton, NC 27520.

⊗ Abstract published in *Advance ACS Abstracts,* October 1, 1996.

[1] Abbreviations: HIV-1, human immunodeficiency virus type 1; TFA, trifluoroacetic acid; HPLC, high performance liquid chromatography; PBS, phosphate buffered saline; UV, ultraviolet; CD, circular dichroism; SVD, singular value decomposition; XLA, Beckman Optima XL-A analytical ultracentrifuge; SE, sedimentation equilibrium; M_w, weight-averaged molecular weight; EC_{50}, 50% effective concentration; Da, daltons; MBP, maltose binding protein; aa, amino acid.

S0006-2960(96)00696-4 CCC: $12.00 © 1996 American Chemical Society

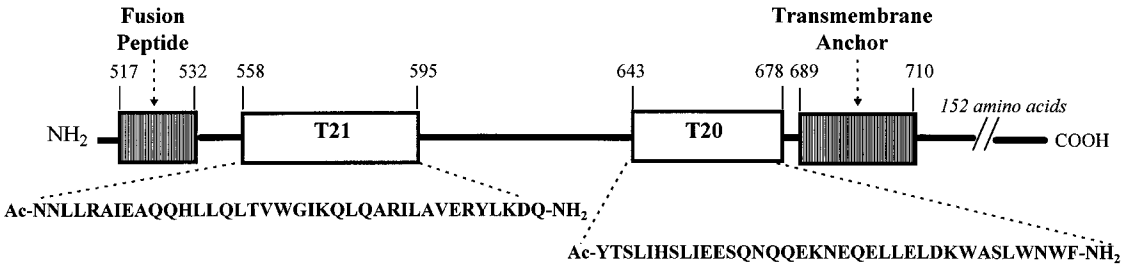

FIGURE 1: Schematic representation of HIV-1_{LAI} gp41.

fusogenic states of the protein (Chen et al., 1995). This paper examines the biophysical properties of these peptides and their interactions to address the roles these peptides and the corresponding gp41 sequences have in the mechanisms of membrane fusion and fusion inhibition. Understanding the process of HIV-1 membrane fusion events and the action of these peptides in disrupting those events will aid our design of potent antiviral compounds for HIV-1 and other viral targets (Lambert et al., 1996).

MATERIALS AND METHODS

Peptide Synthesis and Purification. Peptides were synthesized on a Rainin Symphony Multiplex multiple peptide synthesizer using standard solid-phase synthesis techniques and 9-fluorenylmethoxycarbonyl (Fmoc) protected amino acids (Fields & Noble, 1990). The peptides were blocked at the N-terminus by an acetyl group and at the C-terminus by an amide group. Cleavage of the peptides from the resin (Rink Amide-MBHA resin obtained from Novabiochem Inc., La Jolla, CA) with concomitant removal of side-chain blocking groups was performed using trifluoroacetic acid (TFA) in the presence of thioanisole, water, 1,2-ethanedithiol, and phenol as carbocation scavengers (King et al., 1990). After cleavage, the peptides were precipitated with cold diethyl ether and the precipitate lyophilized and purified. Peptides were purified by reverse-phase HPLC using a Waters DeltaPak C18 column (25 × 300 mm, 15 μm particles) using a water and acetonitrile gradient containing 0.1% (v/v) TFA. All peptides were >95% pure as monitored by analytical HPLC; sample identity was confirmed with electrospray mass spectrometry (Protein Structure Facility, University of Michigan).

Peptide solutions were prepared with buffer containing 100 mM NaCl and 50 mM sodium phosphate (PBS) and adjusted to pH 7 (pH 6 buffer was used for T21 to increase peptide solubility). Peptide concentration of the stock solutions was determined using UV absorbance (Hitachi U-2000) at three wavelengths: 276, 280, and 288 nm (Edelhoch, 1967; Milhalyi, 1968). Dilution of stock solutions to final concentrations as noted in the text were performed in pH 7 PBS.

Analytical Ultracentrifugation. Sedimentation equilibrium experiments were performed on a Beckman Optima XL-A analytical ultracentrifuge at 4 °C (to aid in conserving peptide secondary structure). Six-channel cells (12-mm optical path length) were used with an An-60 Ti rotor operated at 20 000, 25 000, 30 000, 35 000, and 40 000 rpm. The cell radii were scanned using 0.001-cm steps with 10 averages/scan (1, 2, and 4 μM spectra required 99 averages/scan); typically, 2 or 3 wavelengths were used. Data were analyzed using standard Beckman XLA data analysis software (version 1.02 for DOS) and Beckman-Origin software (version 2.01 for Windows). The methods described by Laue et al. (1992) were used to calculate partial specific volumes ($\bar{v}$: T21 = 0.743 mL/g; T20 = 0.717 mL/g) and the solvent density (ρ = 1.0051) at 4 °C; the partial specific volume was held constant for all models considered. The suitability of a particular model (goodness of fit) was judged by the trends observed in the residuals (Johnson et al., 1994). Residuals are obtained by calculating at each radial position the difference between the experimental absorbance and the absorbance calculated by assuming a model which describes the solution species and interactions. Residuals which are randomly distributed about the calculated curve indicate that the model chosen to describe the solution species is consistent with the data. Residuals which show a systematic trend indicate that the chosen model does not correctly describe the solution species and associations.

Single data files were first normalized to 285-nm absorbance values using Beer's law. They were then analyzed using a single ideal species model to determine a weight-averaged molecular weight (M_w). When systematic residuals or a M_w higher than the monomer molecular weight indicated the presence of self-association, several different associative models were investigated, including monomer/trimer, monomer/tetramer, and monomer/dimer/tetramer. The accuracy of SE analyses limits the consideration to a maximum of three solution species in a given model. The single data file analysis provides a good estimate of the choice of the appropriate association model and values for the fitting parameters. A simultaneous, global fitting of multiple data files (at different concentrations and speeds) was then performed to provide the best determination of association constants and 95% confidence intervals. To convert the resulting association constants from absorbance units to concentration units, it was assumed that the absorbance of an *n*-mer is *n* times that of a monomer.

Circular Dichroism. Circular dichroism (CD) spectra were obtained using an AVIV Associates 62DS spectrometer equipped with a thermoelectric temperature controller. Spectra were obtained at 1 °C with 0.5-nm steps from 200 to 260 nm, 1.5 nm bandwidth, and a typical averaging time of 4 s/step. After the cell/buffer blank was subtracted, spectra were smoothed using a third-order least-squares polynomial fit with a conservative (5−10 point) window size to give random residuals. Mixing experiments were performed by comparing the spectrum of the two peptides mixed together in a 1-cm path length cell at the desired concentrations (*experimental spectrum*) to the sum of the individual spectra of the peptides, each solution in a 0.5-cm cell (*theoretical noninteracting spectrum*); details on the conversion to mean residue ellipticity are contained in the legend of Figure 6.

Viral Assays. CEM and Molt-4 cells were maintained in RPMI 1640 with 10% and 20% fetal bovine serum, respectively. Virus was propagated in CEM cells and used to establish chronically infected cells. HIV-1 syncytial assays were performed as described by Matthews et al. (1987).

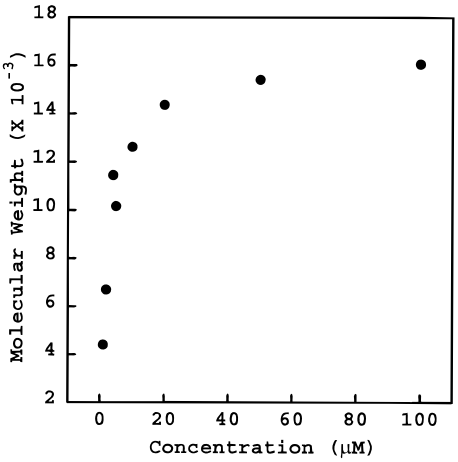

FIGURE 2: Weight-averaged molecular weight for T21 as a function of loading concentration. Data are averages of the results for 20K, 25K, and 30K rpm data. M_w was obtained by fitting the T21 sedimentation equilibrium data to a single ideal species model.

Briefly, uninfected Molt-4 cells (70 000/well of a 1/2 area 96-well plate) were incubated with chronically HIV-1_{LAI} infected CEM cells (10 000/well) for 18−24 h in the presence or absence of peptide. Peptide concentrations were determined by UV spectroscopy as described above. Syncytia comprised of a minimum of 5 cell widths across were enumerated under 400× magnification. Dose response curves were generated and EC_{50} (50% effective concentration) values calculated using the method described by Karber (1931).

RESULTS

Sedimentation Equilibrium Experiments Indicate Monomer/Dimer/Tetramer Equilibrium Established by T21. Sedimentation equilibrium (SE) experiments were performed on T21 using eight different loading concentrations (1−100 μM) and three rotor speeds, yielding 24 data files. The reported results are consistent for two separate sample loadings. The analysis of the data set began with an examination of the individual data files, comparing the various results obtained with different assumptions regarding the peptide solution behavior. Next, a global analysis of the data was performed using the associative model and starting parameters which best reproduced the individual data files. The following paragraphs describe the results obtained from this procedure. Graphical results are presented for the weight-averaged molecular weight vs loading concentration (Figure 2) and the modeling results for the 10 and 100 μM data (Figures 3 and 4), while the results for the global analysis of the data are summarized in Table 1.

Data analysis began by using Beer's law to convert each file to 285 nm absorbance values. The weight-averaged molecular weight (M_w) of T21 as a function of the loading concentration, determined by assuming a single ideal species in solution, is presented in Figure 2. For most of the 24 data files, the systematic trend observed in the residuals indicates that this is not an appropriate model from which to generate detailed conclusions about sample behavior. However, several statements can be made regarding the sample at this point. First, the dramatic rise in M_w which occurs with loading concentration indicates that a self-associating species is an appropriate model to consider. Second, the fact that the M_w for each loading concentration is constant over the three rotor speeds (data not shown) suggests that the system consists of a homogeneous, self-associating species; a heterogeneous noninteracting system would display a marked decrease in M_w with increasing rotor speed (Laue, 1992). Third, although the M_w appears to reach a maximum corresponding to 3.5 times the monomer molecular weight, the systematic residuals suggest that it is premature to use this plot as indicative of nonideality in the sample (which could decrease the apparent molecular weight determined). Such considerations should be made only after attempts to reproduce the data with a simpler model (such as an ideal self-associating species) are exhausted (Johnson et al., 1981).

An individual analysis of each data file can indicate the most appropriate self-association equilibrium to consider for T21. The 1 μM data files (data not shown) produce random residuals when fit with a single ideal species model. A comparison of the resulting M_w of 4400 Da [chi-squared (χ^2) $= 5.31 \times 10^{-8}$, 6.59×10^{-8}, and 7.73×10^{-8} for fitting to the 20K, 25K, and 30K rpm data, respectively, here and subsequent] to the theoretical molecular weight of T21 (4526 Da) predicts that the dominant solution species is monomeric. The 2 μM data files (data not shown) also produce random residuals with a single ideal species model and predict a M_w of 6665 Da ($\chi^2 = 4.76 \times 10^{-8}$, 7.26×10^{-8}, and 7.55×10^{-8}), corresponding to approximately 50% monomer and 50% dimer, assuming two solution species. Due to the signal/noise limitations of these concentration points, these files were not analyzed further.

Analysis of the 4 and 5 μm data files with a single ideal species model produces random residuals (data not shown) and predictions for M_w of 11 500 Da ($\chi^2 = 4.92 \times 10^{-8}$, 4.40×10^{-8}, and 6.34×10^{-8}) and 10 780 Da ($\chi^2 = 1.95 \times 10^{-7}$, 3.48×10^{-7}, and 3.11×10^{-7}), respectively. Since these values correspond to 2.5 times the monomer molecular weight, several self-association equilibria were examined to determine the most appropriate model. Both a monomer/tetramer equilibrium (4 μM $\chi^2 = 5.19 \times 10^{-8}$, 4.92×10^{-8}, and 6.00×10^{-8}; 5 μM $\chi^2 = 1.96 \times 10^{-7}$, 2.24×10^{-7}, and 2.40×10^{-7}) and a monomer/dimer/tetramer equilibrium (4 μM $\chi^2 = 5.03 \times 10^{-8}$, 4.52×10^{-8}, and 5.88×10^{-8}; 5 μM $\chi^2 = 1.91 \times 10^{-7}$, 2.76×10^{-7}, and 2.78×10^{-7}) produce random residuals. A monomer/trimer self-association produces a fit which is adequate (4 μM $\chi^2 = 6.04 \times 10^{-8}$, 4.53×10^{-8}, and 5.88×10^{-8}; 5 μM $\chi^2 = 3.08 \times 10^{-7}$, 3.33×10^{-7}, and 2.99×10^{-7}), yet which shows systematic residuals at the largest radius values. These calculations suggest that the most appropriate model is one which incorporates a tetramer species.

Figure 3 presents the results of calculations considering several models for the 10 μM data at 25K rpm. Analysis of the data files with a single ideal species model produces results with random residuals at 20K rpm ($\chi^2 = 9.78 \times 10^{-8}$) and slightly systematic residuals at 25K ($\chi^2 = 1.88 \times 10^{-7}$, Figure 3A) and 30K rpm ($\chi^2 = 2.5 \times 10^{-7}$); the average M_w from these calculations is 12 560 Da, corresponding to 2.8 times the monomer molecular weight. A monomer/trimer model ($\chi^2 = 2.1 \times 10^{-7}$, 3.45×10^{-7}, and 1.87×10^{-7}) produces systematic error in the residuals (Figure 3B). A monomer/tetramer model (Figure 3C) also produces systematic residuals for all three speeds ($\chi^2 = 1.82 \times 10^{-7}$, 3.57×10^{-7}, and 4.77×10^{-7}); the pattern of these residuals suggests that a species with a molecular weight between that of a monomer and a tetramer could improve the fit. Indeed, when a monomer/dimer/tetramer model is considered, the fit to

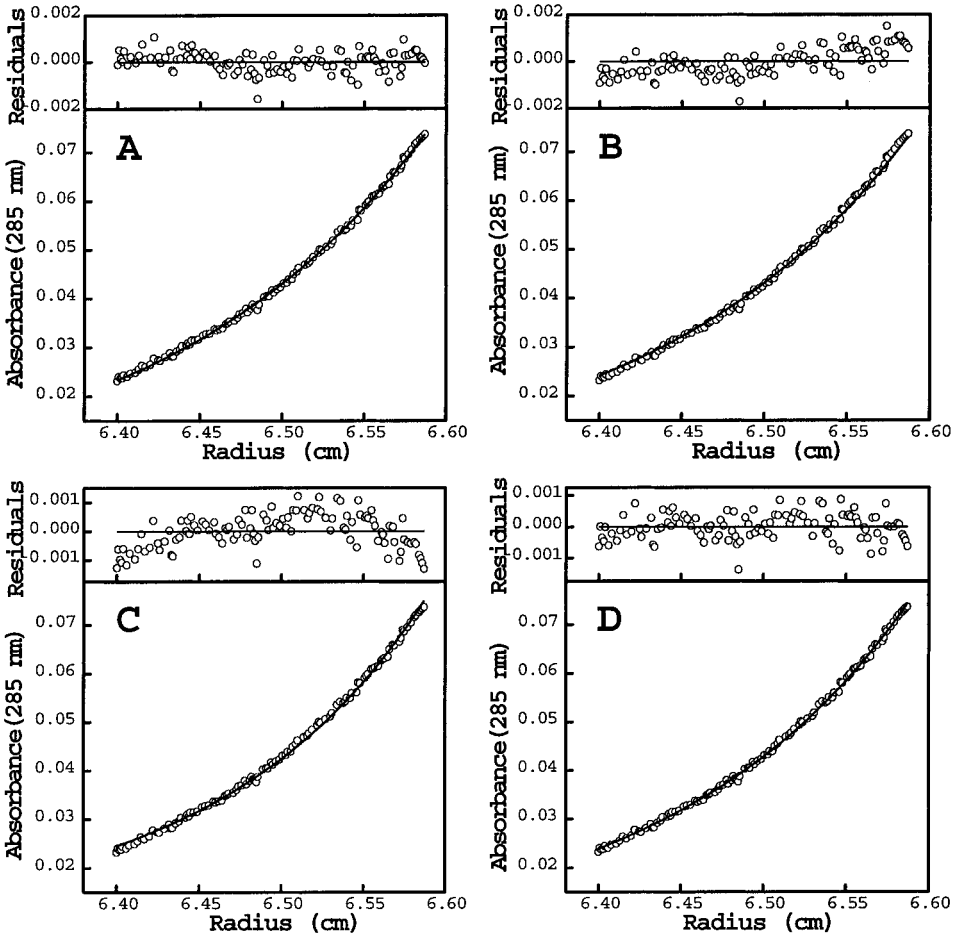

FIGURE 3: Sedimentation equilibrium results at 25 000 rpm, 4 °C, for 10 μM T21. Data was obtained at 205 nm and converted to absorbance at 285 nm for fitting procedures. The results of fitting this single file to four self-association models are superimposed on the data with residuals displayed above. (A) Single ideal species model ($\chi^2 = 1.88 \times 10^{-7}$), $M_w = 12\,560$ Da. (B) Monomer/trimer ($\chi^2 = 3.45 \times 10^{-7}$), $K_{13} = 1.8 \times 10^{12}$ M^{-2}. (C) Monomer/tetramer ($\chi^2 = 3.57 \times 10^{-7}$), $K_{14} = 1.9 \times 10^{16}$ M^{-3}. (D) Monomer/dimer/tetramer ($\chi^2 = 1.78 \times 10^{-7}$), $K_{12} = 1.5 \times 10^{8}$ M^{-1}, $K_{24} = 1.8 \times 10^{5}$ M^{-1}, $K_{14} = 4 \times 10^{22}$ M^{-3}. See Table 1 and text for final results arising from a global fit to multiple data files.

the data in terms of the residuals is significantly improved ($\chi^2 = 1.17 \times 10^{-7}$, 1.78×10^{-7}, and 1.83×10^{-7}). As can be seen in Figure 3D, the residuals produce a random distribution about the calculated curve. These data suggest that the best self-association model to reproduce this data is one which includes both a dimer and a tetramer.

The 20 μM data files (data not shown) produce results very similar to those at 10 μM. The single ideal species model gives systematic residuals for the 20K results ($\chi^2 = 4.03 \times 10^{-7}$) and random residuals for the 25K and 30K results ($\chi^2 = 1.10 \times 10^{-6}$ and 1.17×10^{-6}); the M_w of 14 070 Da corresponds to 3.1 times the monomer molecular weight. As with the 10 μM data, the 20 μM data produces systematic residuals with a monomer/trimer model ($\chi^2 = 3.22 \times 10^{-6}$, 4.64×10^{-6}, and 3.89×10^{-6}) and a monomer/tetramer model ($\chi^2 = 8.36 \times 10^{-7}$, 1.79×10^{-6}, and 1.61×10^{-6}) and gives random residuals when a monomer/dimer/tetramer equilibrium is considered ($\chi^2 = 5.72 \times 10^{-7}$, 1.40×10^{-6}, and 1.61×10^{-6}). Similar results are also obtained with the 50 μM data files (data not shown): a single ideal species model produces systematic residuals ($\chi^2 = 1.22 \times 10^{-5}$, 1.74×10^{-5}, and 2.79×10^{-5}), the monomer/tetramer model produces systematic residuals ($\chi^2 = 2.64 \times 10^{-5}$, 6.95×10^{-5}, and 9.62×10^{-5}), and the monomer/dimer/tetramer model produces the best fit with random residuals ($\chi^2 = 1.31 \times 10^{-5}$, 1.37×10^{-5}, and 1.84×10^{-5}).

The 100 μM data at 25K rpm and modeling results using the four different models are presented in Figure 4. The single ideal species model in Figure 4A produces random residuals ($\chi^2 = 2.83 \times 10^{-5}$, 4.24×10^{-5}, and 5.78×10^{-5}) and a M_w of 15 890 Da, corresponding to 3.5 times the monomer molecular weight. Given this M_w, it is not surprising that the monomer/trimer model (Figure 4B) does not reproduce the data well, as can be seen by the systematic trend in the residuals (χ^2 for 25K data $= 7.86 \times 10^{-5}$). The monomer/tetramer ($\chi^2 = 2.95 \times 10^{-5}$, 4.30×10^{-5}, and 8.67×10^{-5}) and the monomer/dimer/tetramer ($\chi^2 = 2.87 \times 10^{-5}$, 4.28×10^{-5}, and 5.02×10^{-5}) models fit the data equally well, as can be seen in the random residuals in Figure 4C,D. The examination of the data files from 4 to 100 μM indicates that a monomer/dimer/tetramer equilibrium best reproduces the entire data set. These results also provide best guesses for the association constants from which to begin a global analysis of the data.

A global analysis of this data was performed using a monomer/dimer/tetramer equilibrium, starting with the A_0 values for each file (the contribution of monomer absorbance at the reference radius) and the average association constants determined from the individual analysis described above. Due to the Origin software limitation of 10 files for a global analysis, we analyzed the data in two groups (group A = 4, 10, and 100 μM data at 20K, 25K, and 30K rpm; group B = 5, 20, and 100 μM data at 20K, 25K, and 30K rpm). The

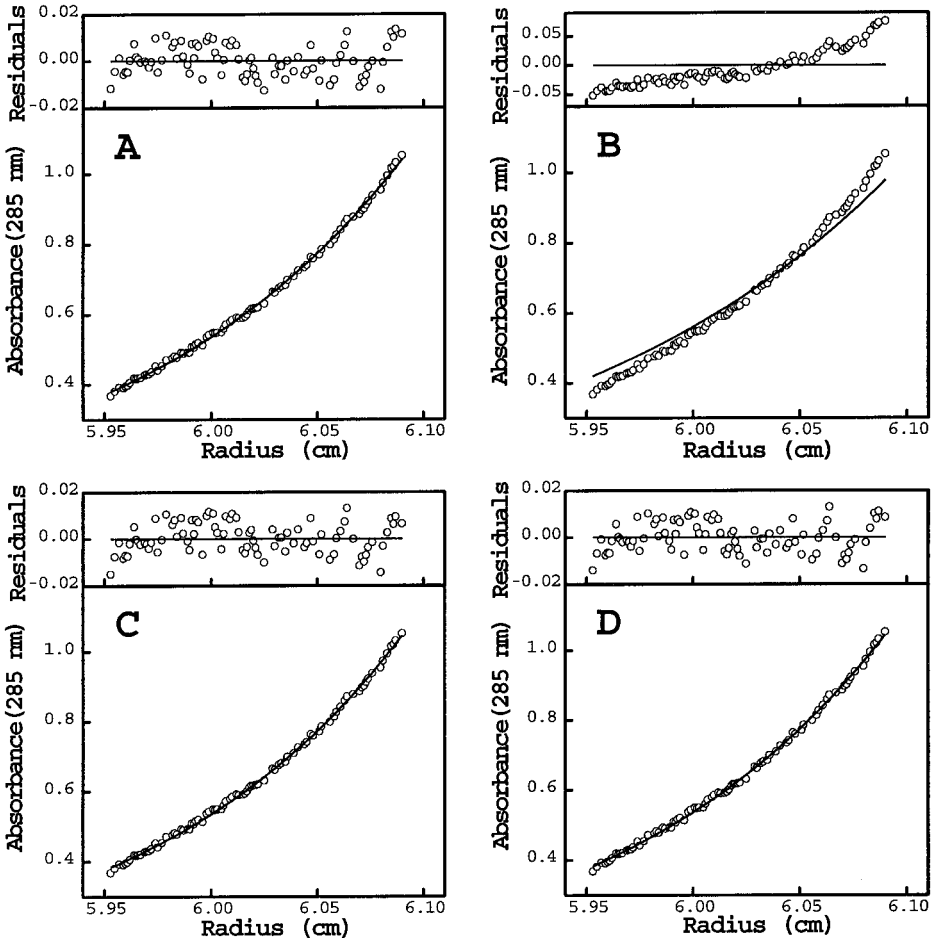

FIGURE 4: Sedimentation equilibrium results at 25 000 rpm, 4 °C, for 100 μM T21. The results of fitting this single file to four self-association models are superimposed on the data with residuals displayed above. (A) Single ideal species model ($\chi^2 = 4.42 \times 10^{-5}$), M_w = 16 210 Da. (B) Monomer/trimer ($\chi^2 = 3.77 \times 10^{-5}$), $K_{13} = 1 \times 10^{19}$ M^{-2}. (C) Monomer/tetramer ($\chi^2 = 4.30 \times 10^{-5}$), $K_{14} = 6 \times 10^{14}$ M^{-3}. (D) Monomer/dimer/tetramer ($\chi^2 = 4.28 \times 10^{-5}$), $K_{12} = 6.2 \times 10^8$ M^{-1}, $K_{24} = 1.8 \times 10^5$ M^{-1}, $K_{14} = 6.8 \times 10^{22}$ M^{-3}. See Table 1 and text for final results arising from a global fit to multiple data files.

initial guesses for the association constants were equal to the averages of the individual file results; equivalent fits were obtained when these parameters were started 2 orders of magnitude higher and lower than these averages. The final results are virtually identical for the two groups and produce a random distribution of residuals for each of the files (goodness of fit = 0.205 and 0.209 for groups A and B, respectively). The association constants and 95% confidence limits are as follows: $K_{12} = 3.42 \times 10^8$ M^{-1} (3.37−3.45) for both groups; $K_{14} = 1.64 \times 10^{22}$ M^{-3} (1.63−1.65) for group A and 1.66×10^{22} (1.65−1.67) for group B. These results produce a $K_{24} = 1.40 \times 10^5$ M^{-1} for group A and 1.42×10^5 M^{-1} for group B. Since the ideal monomer/dimer/tetramer self-association model reproduces the entire T21 data set well, we did not consider adding any additional parameters, such as nonideality, to the model.

Sedimentation Equilibrium Experiments Suggest a Slowly-Equilibrating Tetrameric Self-Association by T20. A sedimentation equilibrium analysis was also performed for the peptide T20 from 1 to 100 μM ($\bar{v} = 0.717$, $\rho = 1.0051$, monomer theoretical molecular weight = 4492 Da). The results were consistent for two independent sample loadings tested at three rotor speeds (30 000, 35 000, and 40 000 rpm). Analyses of the data using a single ideal species model for 1 μM ($\chi^2 = 1.09 \times 10^{-7}$, 1.49×10^{-7}, and 0.92×10^{-7} for the 30, 35, and 40K rpm data, respectively, here and subsequent), 2 μM ($\chi^2 = 3.91 \times 10^{-8}$, 3.55×10^{-8}, and 3.03×10^{-8}), 4 μM ($\chi^2 = 2.74 \times 10^{-7}$, 2.34×10^{-7}, and 2.72×10^{-7}), 5 μM ($\chi^2 = 3.24 \times 10^{-6}$, 2.47×10^{-6}, and 2.05×10^{-6}), and 10 μM data ($\chi^2 = 8.30 \times 10^{-7}$, 6.94×10^{-7}, and 8.37×10^{-7}) produce random residuals with monomeric molecular weights. Representative data and the fitting results for the 10 μM data at 35K rpm are presented in Figure 5A.

The data for the 20 μM ($\chi^2 = 2.12 \times 10^{-6}$, 3.06×10^{-6}, and 3.85×10^{-6}), 40 μM ($\chi^2 = 1.80 \times 10^{-4}$, 2.0×10^{-4}, and 1.80×10^{-4}), 50 μM ($\chi^2 = 1.50 \times 10^{-4}$, 3.10, $\times 10^{-4}$ and 8.7×10^{-4}), and 100 μM ($\chi^2 = 0.84 \times 10^{-3}$, 1.29×10^{-3}, and 1.55×10^{-3}) solutions are not reproduced well using the single ideal species model. As can be seen for the 100 μM data (Figure 5B), systematic residuals result, suggestive of a self-association. The remaining panels present the results using two associative models to reproduce the 100 μM data: a monomer/trimer (Figure 5C) and a monomer/tetramer model (Figure 5D). These results indicate that the monomer/tetramer model ($\chi^2 = 1.50 \times 10^{-4}$, 1.9×10^{-4}, and 1.7×10^{-4}) is more appropriate for describing a T20 self-association; the monomer/trimer model ($\chi^2 = 4.4 \times 10^{-4}$, 5.2×10^{-4}, and 5.1×10^{-4}) produces a systematic deviation in the residuals. Similar results are obtained for the 20, 40, and 50 μM data files. The association constants for a monomer/tetramer equilibrium arising from fitting the individual data files range from 1.80×10^{11} M^{-3} to 1.10×10^{12} M^{-3}. These association constants show no specific trend

Table 1: Sedimentation Equilibrium Results for T21

[T21] (μM)	T21[a] predominant solution species	model	M_w from single ideal species model	pattern of residuals	χ^2 values 20 K rpm	25 K rpm	30 K rpm
1	monomer/dimer	single ideal species	4 400 Da	random	5.31×10^{-8}	6.59×10^{-8}	7.73×10^{-8}
2	monomer/dimer	single ideal species	6 460 Da	random	4.76×10^{-8}	7.26×10^{-8}	7.55×10^{-8}
4	monomer/dimer/tetramer	single ideal species	11 100 Da	random	4.92×10^{-8}	4.40×10^{-8}	6.34×10^{-8}
		monomer/trimer		systematic	6.04×10^{-8}	4.53×10^{-8}	5.88×10^{-8}
		monomer/tetramer		random	5.19×10^{-8}	4.92×10^{-8}	6.00×10^{-8}
		monomer/dimer/ tetramer		random	5.03×10^{-8}	4.52×10^{-8}	5.88×10^{-8}
5	monomer/dimer/tetramer	single ideal species	10 780 Da	random	1.95×10^{-7}	3.48×10^{-7}	3.11×10^{-7}
		monomer/trimer		systematic	3.08×10^{-7}	3.33×10^{-7}	2.99×10^{-7}
		monomer/tetramer		random	1.96×10^{-7}	2.24×10^{-7}	2.40×10^{-7}
		monomer/dimer/ tetramer		random	1.91×10^{-7}	2.76×10^{-7}	2.78×10^{-7}
10	dimer/tetramer	single ideal species	12 560 Da	systematic	9.78×10^{-8}	1.88×10^{-7}	2.50×10^{-7}
		monomer/trimer		systematic	2.10×10^{-7}	3.45×10^{-7}	1.87×10^{-7}
		monomer/tetramer		systematic	1.82×10^{-7}	3.57×10^{-7}	4.77×10^{-7}
		monomer/dimer/ tetramer		random	1.17×10^{-7}	1.78×10^{-7}	1.83×10^{-7}
20	dimer/tetramer	single ideal species	14 070 Da	systematic	4.03×10^{-7}	1.10×10^{-6}	1.17×10^{-6}
		monomer/trimer		systematic	3.22×10^{-6}	4.64×10^{-6}	3.89×10^{-6}
		monomer/tetramer		systematic	8.36×10^{-6}	1.79×10^{-6}	1.61×10^{-6}
		monomer/dimer/ tetramer		random	5.72×10^{-7}	1.40×10^{-6}	1.61×10^{-6}
50	dimer/tetramer	single ideal species	15 340 Da	systematic	1.22×10^{-5}	1.74×10^{-5}	2.79×10^{-5}
		monomer/trimer		systematic	3.51×10^{-5}	4.64×10^{-5}	8.92×10^{-5}
		monomer/tetramer		systematic	2.64×10^{-5}	6.95×10^{-5}	9.62×10^{-5}
		monomer/dimer/ tetramer		random	1.31×10^{-5}	1.37×10^{-5}	1.84×10^{-5}
100	tetramer	single ideal species	15 890 Da	random	2.83×10^{-5}	4.24×10^{-5}	5.78×10^{-5}
		monomer/trimer		systematic	4.23×10^{-5}	7.86×10^{-5}	9.57×10^{-5}
		monomer/tetramer		random	2.95×10^{-5}	4.30×10^{-5}	8.67×10^{-5}
		monomer/dimer/ tetramer		random	2.87×10^{-5}	4.28×10^{-5}	5.02×10^{-5}

[a] Sedimentation equilibrium data for T21 were analyzed using a monomer molecular weight = 4526 Da, $\bar{v} = 0.743$ mL/g, and $\rho = 1.0051$ g/mL. Methods of analysis are described in the text. The association constants resulting from a weighted global fit (goodness of fit = 0.207) of the data using a monomer/dimer/tetramer equilibrium are $K_{12} = 3.42 \times 10^8$ M^{-1} (95% confidence interval = (3.37−3.45) $\times 10^8$ M^{-1}), $K_{14} = 1.65 \times 10^{22}$ M^{-3} ((1.63−1.66) $\times 10^{22}$ M^{-3}), $K_{24} = 1.41 \times 10^5$ M^{-1} ((1.40−1.44) $\times 10^5$ M^{-1}). The predominant solution species arise from a global analysis of the sedimentation equilibrium data (the association constants) and from the analysis of the individual data files (those solution species required to reproduce the data at a given concentration).

with increasing rotor speed, suggesting that a reversible self-association is an appropriate model for this peptide (McRorie & Voelker, 1993).

A global fit of the data files was then attempted, using a monomer/tetramer equilibrium and starting parameters as determined in the individual data file analysis. However, we were unable to find a set of parameters using a monomer/tetramer association which would produce truly random residuals for the entire data set. The best attempt, considering the 40 and 50 μM data files at 30K, 35K, and 40K rpm, converged to a result with an association constant equal to 3.25×10^{11} M^{-3} [95% confidence interval = (3.01−3.51) $\times 10^{11}$ M^{-3}]. However, this calculation (goodness of fit = 5.23) produces both random residuals (30K rpm data) and residuals with systematic trends suggestive of requiring less (35K rpm data) and more (40K rpm data) emphasis on the associating species. This suggests that an ideal, reversible self-associating species may not be the appropriate model for this peptide.

Another observation which supports this suggestion is the fact that the weight-averaged molecular weight for T20 decreases with increasing rotor speeds; this is suggestive of heterogeneity in the sample (Laue, 1992). Yphantis et al. (1978) have described five sources of heterogeneity in sedimentation equilibrium experiments: (1) the presence of contaminating solutes with a molecular weight different than that of the sample, (2) the presence of different chemical forms of the self-associating solute with different association constants, (3) the presence of irreversible aggregates of the main component, (4) the presence of "incompetent monomer" incapable of self-association, and (5) the presence of metastable conformers of the self-associating solute that are not in rapid equilibrium with each other over the time course of the experiment and that exhibit differing association behavior.

Sources 1 and 2 can be ruled out since the purity of this sample is 98% (HPLC) and amino acid analysis and mass spectrometry have confirmed sample identity; therefore, it is unlikely that contaminating solutes or different chemical forms of the peptide are the cause of this phenomenon. It is also unlikely that irreversible aggregates are the cause of this heterogeneity (source 3) since the 1−10 μM data are reproduced well with a monomeric species, and the 20−100 μM data are not, while all samples were prepared from the same stock solution. One would expect irreversible aggregation to affect the low concentations as well as the high concentrations. Rather, it is more likely that several metastable conformers of the T20 peptide are present in solution, at least one of which exhibits a self-association equilibrium. The heterogeneity suggested by the analysis described above could be due to a slow interconversion of a conformer from an "incompetent monomer" structure to a structure capable of self-association as a tetramer (sources 4 and 5). As discussed below, the CD spectrum of T20 indicates that this peptide does not adopt a well-defined secondary structure in solution (20% helicity content), making this explanation plausible. These observations are suggestive of complicated solution behavior at concentrations greater than 20 μM. However, at concentrations less than 20 μM, we can say with good certainty that the predominant solution species of T20 is monomeric peptide, since these data points were reproduced well with a single species in solution corresponding to monomeric molecular weight.

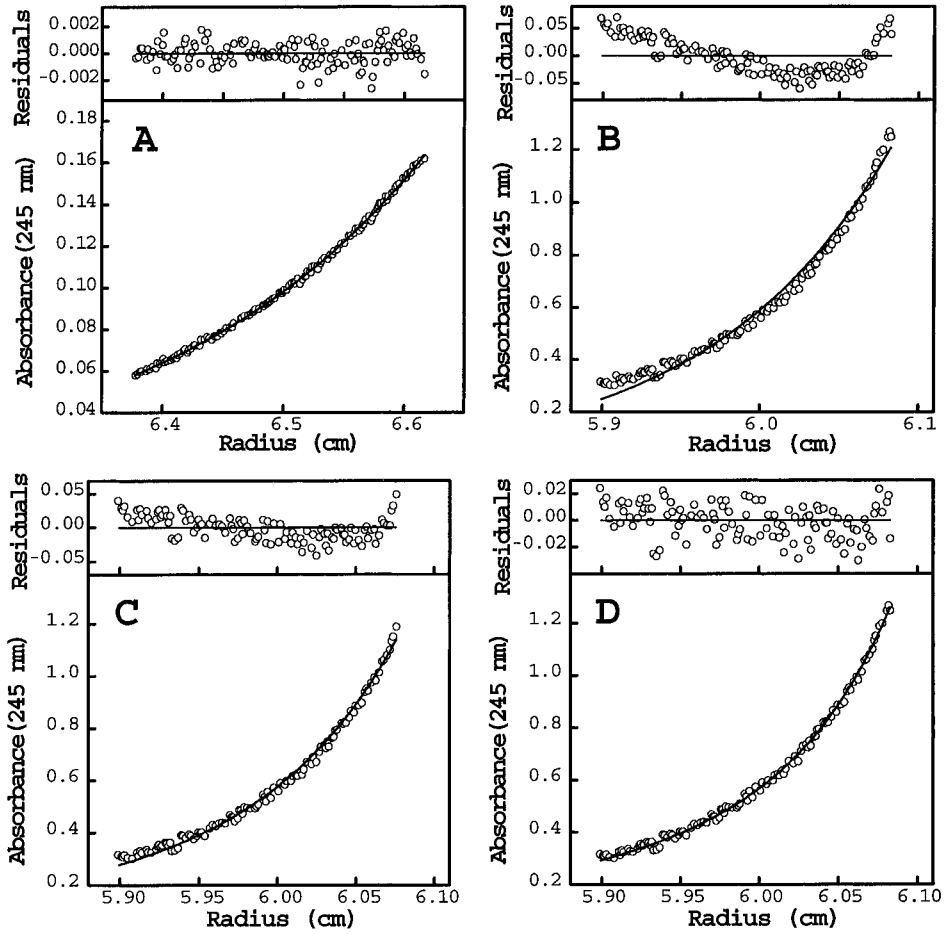

FIGURE 5: Sedimentation equilibrium results at 35 000 rpm, 4 °C, for 10 μM and 100 μM T20. The results of fitting to three self-association models are superimposed on the data with residuals displayed above. (A) 10 μM T20; single ideal species model ($\chi^2 = 6.94 \times 10^{-7}$), M_w = 4000 Da. (B) 100 μM T20; single ideal species model ($\chi^2 = 1.3 \times 10^{-3}$), M_w = 8400 Da. (C) 100 μM T20; monomer/ trimer ($\chi^2 = 5.2 \times 10^{-4}$), $K_{13} = 2 \times 10^8$ M^{-2}. (D) 100 μM T20; monomer/tetramer ($\chi^2 = 1.9 \times 10^{-4}$), $K_{14} = 1 \times 10^{12}$ M^{-3}.

CD Experiments Investigating Peptide Interactions Show Correlation to Antiviral Results. Figure 6A presents the individual CD spectra of the peptides T21 and T20. The CD spectrum of T21 has minima at 222 and 208 nm, indicating that the peptide has significant helical character, while the T20 spectrum is indicative of significantly less helical character (Holzwarth & Doty, 1965). Deconvolution of these spectra using single value decomposition (SVD) with a basis set of 33 protein spectra (Johnson, 1990) predicts the fraction of helix of these peptides to be 90% and 20%, respectively. Identical results are also obtained using LINCOMB, an algorithm which computes a linear combination using five peptide basis spectra (Perczel et al., 1992). The helicity content of the coiled-coil peptide T21 is expected to be decreased by 10% from the actual value due to the modulation of the CD signal arising from interactions between helices (Manning, 1989).

Figure 6 also presents the results of CD mixing experiments which investigate structural changes resulting from peptide interactions. If two peptides do not interact with each other, and therefore no structural change occurs, the "theoretical, noninteracting" and "experimental" spectra (defined in Materials and Methods) will be identical (for example, panel C of Figure 6). However, if two peptides do interact, resulting in a structural change of the components, these CD spectra will be different. Panel B shows the results of a CD mixing experiment of 10 μM T21 and 10 μM T20. A dramatic difference between the two spectra is evident, indicating that the two peptides interact to produce a structural change when mixed in the same solution. Analysis of the theoretical, noninteracting spectrum yields a prediction of 60% helicity content, corresponding to the average of the helical content of the individual peptides. The experimental spectrum of the mixed peptides displays a fine precipitate suspension and produces a spectrum having a broad well, centered at 225 nm, and a shoulder at 210 nm. In addition to including the circular differential absorption of the solution, this spectrum may also include contributions from circular differential scattering arising from the fine precipitate in solution (Bustamante, 1983). The present experiment does not distinguish between the two phenomena, but does serve as a qualitative indicator that significant structural changes have occurred as a result of mixing the two peptides in solution.

Panel C explores the specificity of this T20−T21 interaction. The mixing of T20 with a peptide from the coiled-coil sequence of GCN4 (Lumb et al., 1994) shows no structural change indicative of an interaction between these two peptides. Identical results are obtained (data not shown) when T20 is mixed with T91, a coiled-coil peptide designed by Hodges and co-workers (Monera et al., 1993). This evidence indicates that T20 interacts in a specific fashion with the T21 coiled-coil peptide sequence from gp41 and requires more than a generic amphipathic coiled-coil interface. This suggests that the inhibitory action of T20 against membrane fusion may involve the specific interaction with the T21 region of gp41 (see Discussion).

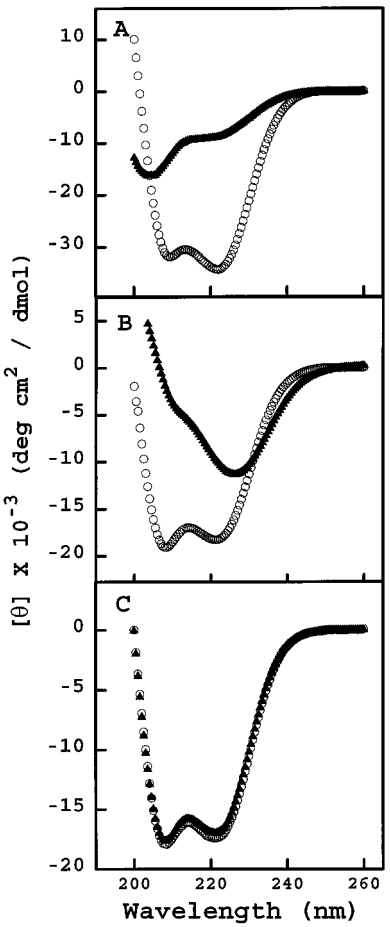

FIGURE 6: Circular dichroism spectra. (A) Open circles (○), 10 μM T21; black triangles (▲), 10 μM T20. (B) Open circles (○), *theoretical noninteracting spectrum* of a mixture of 10 μM T21 and 10 μM T20. Black triangles (▲), *experimental spectrum* of a mixture of 10 μM T21 and 10 μM T20 in 1 cm path length cell. (C) Open circles (○), *theoretical noninteracting spectrum* of a mixture of 10 μM GCN4 peptide and 10 μM T20. Black triangles (▲), *experimental spectrum* of a mixture of 10 μM GCN4 peptide and 10 μM T20 in 1-cm path length cell. To obtain the *theoretical noninteracting spectrum* for the mixing experiments (panels B and C), the raw CD spectra in 0.5-cm cells of 10 μM T21 (or 10 μM GCN4 peptide) and 10 μM T20 were summed; then, the mean residue ellipticity conversion was performed, assuming an average peptide length of 37 residues for T21/T20 (or 35 residues for GCN4 peptide/T20), a 10 μM peptide concentration, and a 1-cm path length. The experimental spectrum for the mixing experiments was obtained by conversion to mean residue ellipticity using the same multiplication factors.

Table 2 presents data demonstrating the dependence of the T20−T21 structural interaction on peptide concentration, length, and amino acid sequence. Each of these peptides produces a CD spectrum similar to that of T20, with the helicity content in the range of 10−20%. The first entry describes the concentration dependence of the T20−T21 interaction. The structural interaction occurs between the two peptides at both a 10:10 and 10:50 μM concentration ratio (T20:T21). Little to no structural interaction occurs at a 1:1 and 1:5 μM ratio. To define what region of T20 is necessary for this structural interaction, several peptides corresponding to truncations of T20 were examined. Identical results are observed for the first two truncation peptides, T715 and T716, indicating that the three N-terminal residues (YTS) are not essential in producing this structural interaction. Further truncations of the N-terminal residues LI (T719) and HS (T712) destroy the ability of the peptide to interact with T21 at a 10:10 μM ratio, although the 10:50 μM structural interaction is preserved. Truncation of additional N-terminal residues (LIEES, T914; QNQQEK, T102; and NEQEL, T221) completely eliminates the ability of the peptide to interact with T21 at any concentration ratio tested. The C-terminal truncated peptide T700 displays no structural interaction with T21. The T714 truncation peptide also does not interact with T21 at any concentration ratio tested; the only difference between this and its "parent" peptide T716 (which interacts with T21 to the same degree as T20) is the truncation of the C-terminal residues WNWF. The lack of interaction of T700 (truncated at the C-terminus) and T714 (truncated at both the N- and C-termini) with T21 suggests that a full or near-full length peptide may be important for this specific interaction to occur.

The ability of these truncation peptides to interact with T21 shows a striking correlation to antiviral activity. Those peptides which interact with T21 at both a 10:10 and 10:50 μM ratio (T20, T715, T716) show potent antiviral activity when tested in fusion assays, with EC_{50} values of approximately 1 ng/mL. Those peptides which display high ng/mL EC_{50} (T719, T712) show a structural interaction at only a 10:50 μM ratio. The remaining peptides of the truncation series (T914, T102, T221, T700, T714) show no structural interaction with T21 and have EC_{50} values greater than 10^4 times higher than that of T20.

Point substitutions of the T20 sequence provide additional information regarding the importance of specific residues in facilitating the structural interaction and the relation of this interaction to antiviral activity. Substitution of the C-terminal sequence WNWF with ANAA (T229) prevents the peptide from structurally interacting with T21 at any concentration ratio, and the peptide is found to be inactive in viral fusion assays. Substitutions in the C-terminal portion of the peptide do not affect the structural interaction at any concentration ratio, although they can affect the antiviral activity. The single proline substitution L→P (T705) has no effect on the structural interaction ability or viral fusion activity of the peptide, while the single proline substitution W→P (T704) maintains the structural interaction capability while decreasing the antiviral potency by 1000-fold. These proline substitutions are analogous to those investigated in the full length gp41 protein (Cao et al., 1993) and show no effect on the ability of the peptide to interact with T21, yet large differences in activity are observed.

DISCUSSION

Peptide T21 Establishes a Monomer/Dimer/Tetramer Equilibrium in Solution. We have shown that the peptide T21 in solution at neutral pH follows a monomer/dimer/tetramer self-association equilibrium. T21 forms a significant amount of tetramer species at concentrations as low as 10 μM. This result confirms and extends earlier predictions based on CD results that this peptide forms a coiled coil under these conditions (Wild et al., 1992). What is surprising is that this peptide retains 90% helicity content at 1 μM, where SE analyses suggest that both monomer and dimer are present in solution. The results from these experiments performed on a range of T21 concentrations (1−100 μM) generally agree with a recent SE study on this peptide performed at 20 and 50 μM (Rabenstein & Shin, 1995). In that study, a monomer/tetramer equilibrium was proposed, although our results require the addition of a dimeric species to accurately reproduce the 10, 20, and 50 μM data. Our

Table 2: Peptide Sequences, CD Mixing, and Antiviral Results[a]

Peptide	Sequence	CD Mixing Results[b] [Peptide] : [T21] (μM) 1 : 1	1 : 5	10 : 10	10 : 50	Anti-Viral Activity[c] EC_{50} (μg/ml)
T20 (DP178)	Ac-YTSLIHSLIEESQNQQEKNEQELLELDKWASLWNWF-NH2	-	+	++	++	0.0005
Truncations						
T715	Ac- TSLIHSLIEESQNQQEKNEQELLELDKWASLWNWF-NH2	-	-	++	++	0.0003
T716	Ac- LIHSLIEESQNQQEKNEQELLELDKWASLWNWF-NH2	-	-	++	++	0.0005
T719	Ac- HSLIEESQNQQEKNEQELLELDKWASLWNWF-NH2	-	-	-	++	0.060
T712	Ac- LIEESQNQQEKNEQELLELDKWASLWNWF-NH2	-	-	-	++	0.110
T914	Ac- QNQQEKNEQELLELDKWASLWNWF-NH2	-	-	-	-	110
T102	Ac- NEQELLELDKWASLWNWF-NH2	-	-	-	-	65
T221	Ac- LELDKWASLWNWF-NH2	-	-	-	-	20
T700	Ac-YTSLIHSLIEESQNQQEKNEQEL -NH2	-	-	-	-	100
T714	Ac- LIHSLIEESQNQQEKNEQELLELDKWASL -NH2	-	-	-	-	10
Substitutions						
T229	Ac-YTSLIHSLIEESQNQQEKNEQELLELDKWASL **ANAA**-NH2	-	-	-	-	>100
T705	Ac-YTSLIHSLIEESQNQQEKNEQELLELDKWASP**W**NWF-NH2	-	-	++	++	0.003
T704	Ac-YTSLIHSLIEESQNQQEKNEQELLELDK**P** ASLWNWF-NH2	-	-	++	++	0.150

[a] Sequences of control coiled-coil peptides referred to in text include: GCN4 peptide = Ac-RMKQLEDKVEELLSKNYHLENEVARLKKLVGER-NH_2; T91 = Ac-KLEALEGKLEALEGKLEALEGLKEALEGKLEALEGK-NH_2. [b] The results of CD mixing experiments are presented with the following designations: A negative sign (−) indicates experiments in which no difference exists between the theoretically and experimentally mixed peptides (i.e., Figure 6C). A single positive sign (+) indicates that a small difference in the CD signal was detected (slight difference in the magnitude of the CD signal, with no change in shape). A double positive sign (++) indicates experiments in which a large difference in the CD spectra is observed (a large difference in magnitude and shape of the CD signal, i.e., Figure 6B). [c] Antiviral fusion assay results are the average of at least two separate experiments. Activity values range 2−3-fold over the values indicated.

results are also consistent with two analyses of recombinant forms of a slightly longer peptide containing the T21 sequence fused to either maltose binding protein (Shugars et al., 1996) or a fragment of protein A (Eric Hunter, personal communication). These studies demonstrated that the peptide establishes a monomer/tetramer equilibrium in solution even when fused to large proteins which are monomeric in their native states.

The finding that the peptide T20 may also exist in a monomer/tetramer equilibrium in solution at concentrations greater than 20 μM is novel. These results are corroborated by CD findings which show a modest increase in helicity content of T20 with increasing concentration, although noncooperative heat denaturation and a constant melting temperature over the concentration range 1−50 μM suggest a weak association (M. K. Lawless, unpublished results). The marginal stability of this association could be due to the breaks in the hydrophobic heptad repeat sequence which could cause a weak association of coils (Cohen & Parry, 1986).

The oligomerization of gp41 in its native and fusogenic states has been debated (Earl et al., 1990; Gelderblom et al., 1987; Owens & Compans, 1990; Pinter et al., 1989; Poumbourios et al., 1992, 1995; Schawaller et al., 1989; Thomas et al., 1991). It has been suggested by mutational studies of intact gp41 that the hydrophobic heptad repeat region of this protein defined by T21 is not involved in the gp41 oligomerization, yet the preservation of the heptad repeat region (and thus its tendency to form coiled coils) is an essential component of a fusion competent protein (Chen et al., 1993; Dubay et al., 1992). It would be interesting to see if mutations within the T20 domain of gp41 could affect the oligomerization of this protein. The possible fusogenic role of the tetrameric oligomerization of both peptides within gp41 will be discussed below.

The results of our experiments appear to contrast with those of a recent publication by Lu et al. (1995). In that study, the authors examined a recombinant protein fragment of gp41 which was resistant to proteolytic digestion. Purification of this fragment revealed two peptides, C-43 (5560 Da) and N-51 (5940 Da) corresponding roughly to the T20 and T21 domains presented in this study. The authors conclude that this complex is a trimer of antiparallel heterodimers, with the N-51 peptide (T21-like) forming a trimeric inner core. Our study of the T21 peptide demonstrates that, over a wide range of concentrations (1−100 μM), a monomer/dimer/tetramer equilibrium is the only model which accounts for the SE results, and that the assumption of a monomer/trimer equilibrium results in systematic error, indicating that a trimer model is not appropriate for this peptide (see Figures 3 and 4). Therefore, these data are not consistent with the results obtained by Lu et al. Several differences between the experimental methods should be noted. First, the two sets of peptide sequences investigated are not identical: N-51 contains 24 C-terminal residues not found in T21, while C-43 contains 15 residues N-terminal to T20 and is missing 7 C-terminal residues. Second, our peptides are synthesized with blocked ends (Table 2), while the digestion of a recombinant protein fragment would leave the N-51 and C-43 peptides with unblocked ends. This difference could have an important effect on peptide structure and interactions in solution (Shoemaker et al., 1987). These sequence differences are important to note when comparing results. Evidence that the sequence differences can lead to differences in structure is found in CD heat denaturation experiments, in which T21 shows a cooperative heat denaturation curve with a $T_m \sim 70$ °C (Wild et al., 1992), while N51 shows a noncooperative heat denaturation (Lu et al., 1995).

CD Mixing Experiments Indicate a Structural Interaction between T20 and Tetrameric T21. Evidence for the T20−T21 structural interaction has been suggested by a variety of experiments (Chen et al., 1995; Lu et al., 1995; Matthews et al., 1994; Neurath et al., 1995; Wild et al., 1994b, 1995).

The results of CD mixing experiments between T20, T715, T716, T719, T712, and T21 at 10:10 μM ratios (Table 2) agree with those of an earlier study which reported raw ellipticity CD spectra for experiments performed at a single concentration (Wild et al., 1995). However, we have demonstrated that the establishment of a structural interaction is critically dependent on the concentration of T21 chosen for the experiment.

CD mixing results show that a structural interaction between T20 and T21 occurs at a 10:10 and 10:50 μM concentration ratio, while little or no structural interaction is observed at a 1:1 and 1:5 μM ratio. In addition, no structural interaction is observed at a 10:1 μM ratio (data not shown), suggesting that the interaction is not dependent on mass action, but on structural differences present at the different concentrations. T20 is monomeric in solution at both 1 and 10 μM; therefore, its involvement in these experiments is constant for the four different conditions. In contrast, T21 is present at different association states under these conditions. The SE results (Table 1) demonstrate that the predominant T21 solution species is a tetramer at 10 and 50 μM. However, at 1 and 5 μM, only a minor amount of tetramer ($\sim$nM range) is present. Thus, the observation of an interaction between T20 and T21 by CD depends exclusively on the concentration and, accordingly, the oligomerization state of T21. *This suggests that the ability of T20 to interact with T21 necessitates the presence of T21 in a tetrameric species.* If T20 could interact with a dimeric T21, a strong structural change would be observed at 5 μM T21. Also, the structural change resulting at 50 μM T21 would be diminished from that observed at 10 μM, since as the concentration increases, fewer dimers and more tetramers of T21 are present. The experimental observation that the extent of structural interaction is greater at the higher concentrations indicates that the interaction depends on the T21 species present at the higher concentrations. The SE results show that this species is tetrameric T21.

Correlation of Structural Interactions with Antiviral Results. The T20 truncation results (Table 2) suggest a requirement for a minimum peptide length necessary to interact with the tetrameric coiled coil. The removal of 1 or 3 N-terminal residues from T20 (T715, T716) has no effect on the peptide's ability to interact with T21 or inhibit membrane fusion. The removal of 5 or 7 N-terminal residues from T20 (T719, T712) prevents the peptide from inducing a structural interaction when mixed with 10 μM T21, while the structural change is clearly evident at 50 μM. Correspondingly, these peptides show diminished antiviral activity. The loss of 12 or more N-terminal residues destroys the structural interaction ability and antiviral activity of the remaining peptide sequence. The structural interaction is not observed even at high concentrations of T21, where the tetramer species predominates. This truncation series suggests a strong correlation between the observation of a structural interaction between a particular peptide and T21 and the antiviral activity of that peptide.

Substitutions in the T20 peptide sequence provide further information on the sequence dependence of this structural interaction and its correlation with antiviral activity. The peptide T229 containing the sequence ANAA in place of WNWF is inactive in fusion assays and demonstrates no interaction with T21 at any concentration tested. This result suggests the importance of the bulky hydrophobic WNWF region for interaction with the T21 sequence. This result is also supported by results with T714, in which removal of the same 4 residues has the same effect. The leucine $\rightarrow$ proline substitution in T705 has no effect on the peptide's ability to interact with T21, nor its ability to inhibit membrane fusion. The typical effect of proline is to introduce "kinks" or distort the secondary structure of a peptide chain, thus halting the propagation of a regular helical structure; this result suggests that a regular helical structure in this region of the peptide may not be critical for binding or activity.

The tryptophan $\rightarrow$ proline mutation in T704 dramatically lowers the antiviral activity of the peptide, while still preserving its ability to interact structurally with T21. *These results suggest that the structural interaction of peptides with T21 is necessary but not sufficient for antiviral activity; amino acid side chains not involved in the specific binding to T21 are needed for the antiviral activity.* Further studies are underway to investigate these findings.

Correlation of Peptide and Protein Structure. Several studies have demonstrated that simplifying protein−protein interaction questions by examining peptides corresponding to sequences within those proteins can give insight to the structure and mechanism of these systems. The study of short peptides from the influenza HA protein led to a prediction of the trimeric coiled-coil state involving the peptide sequences within the native protein; these predictions were later confirmed by X-ray crystal structures (Bullough et al., 1994; Carr & Kim, 1993; Wilson et al., 1981). A study of a 23-residue peptide from the yeast transcription factor GCN4, which was shown by X-ray crystallography to form a coiled-coil structure, demonstrated that the synthetic peptide adopts a coiled-coil structure in solution (Lumb et al., 1994; O'Shea et al., 1991). Additional studies have demonstrated that peptide fragments can fold into the native complexes found in the corresponding proteins (Kim & Baldwin, 1990; Kippen et al., 1994; Tasayco & Carey, 1992). The ability of a T21-like peptide to form tetramers even when fused to maltose binding protein or a protein A fragment suggests that the results of studying the T21 peptide are applicable to the T21-like domain of gp41 (Shugars et al., 1996; Eric Hunter, personal communication). We therefore describe the possible roles that the T20 and T21 sequences of gp41 play in the native protein based on the structural information of the peptides in solution.

Implications for the Mechanism of Membrane-Fusion Inhibition. T21 and T20 are two peptides with sequences taken from HIV-1 gp41 which show remarkable inhibition of viral fusion (Wild et al., 1992, 1993, 1994a,b). It has been proposed that the inhibitory activity of each peptide arises from interactions with the other peptide's sequence within gp41 (Matthews et al., 1994). Yet it is not understood why the EC_{50} value of T20 is 1000-fold less than that of T21 in fusion assays. The results described in this study suggest a possible explanation. These data indicate that T21 must be present in its tetrameric form to interact with T20. The antiviral action of T20 presumably occurs through its interacting with the tetrameric coiled-coil structure established by the T21-like domain in the fusogenic state of gp41, as indicated by the T21 interaction with T20. This is possible at very low concentrations since monomeric T20 can interact with the tetrameric structure formed by the T21 sequence. In contrast, the T21 peptide must be present at concentrations high enough to form sufficient tetrameric species to interact with the T20 sequence in gp41. A predominance of T21

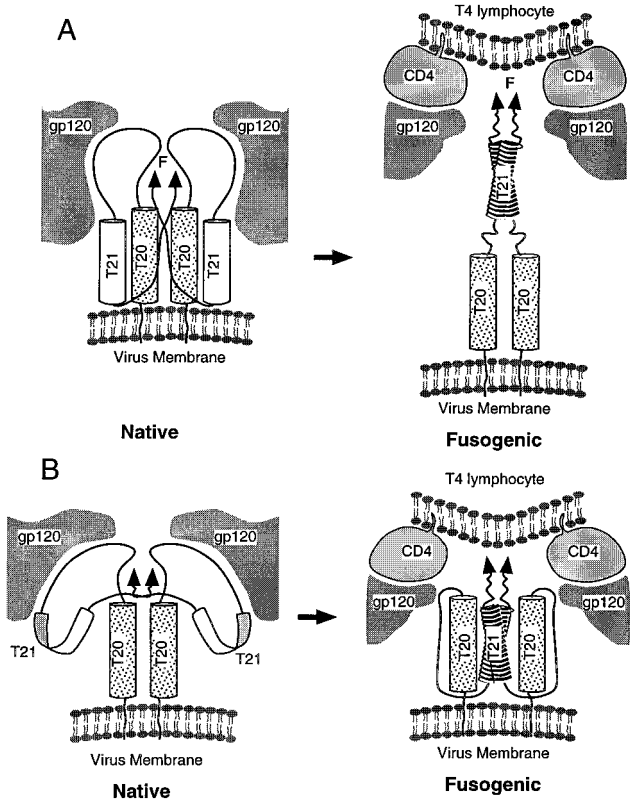

FIGURE 7: Models of membrane fusion proposed by Matthews et al. [adapted from Matthews et al. (1994)]. For clarity, a dimer of gp41/120 is presented. In both models, the coiled-coil structure of the gp41 domain corresponding to T21 is established in the fusogenic state. In model A, the interaction between the T20 and T21 domains occurs in the native state between monomers. In model B, the interaction between the two domains occurs in the fusogenic state after the coiled-coil structure has been established.

tetrameric species is seen in the XLA data only at concentrations equal to or higher than 10 μM. The lowest T21 concentration reliably detectable with the XLA is 1 μM; at that concentration, the data indicate a T21 monomer in solution. However, higher order oligomers from the equilibrium could be present at concentrations up to ~10% and not be detected by this method (McRorie & Voelker, 1993). Since the 2 μM concentration is where we begin to detect higher order species, it is likely that the presence of a small amount of tetrameric T21 at the EC_{50} concentration (0.2−1 μM) is responsible for the activity of this peptide. Previous evidence of a 5-fold decrease in the EC_{50} value upon dimerization of the T21 peptide supports this result, since dimerization would allow the formation of tetrameric T21 at lower concentrations (Wild et al., 1992). These results contribute to the growing understanding of the mechanism of action of potent antiviral peptide inhibitors.

Implications for the Mechanism of Membrane Fusion. These results support models of membrane fusion which involve an interaction between the T20 domain of gp41 and a tetrameric coiled coil established by the T21 domains of tetrameric gp41. These results are not consistent with models suggesting that the fusogenic state is a trimer of dimers (Lu et al., 1995). Our results are consistent with one of two models proposed by Matthews et al. for the structural changes associated with HIV membrane fusion (Matthews et al., 1994). These models have been adapted in Figure 7. For clarity, a dimer of gp41/120 heterodimers is presented, although we will discuss structural changes in terms of a tetrameric oligomerization state. Both models include: (1) a native state held together by noncovalent protein−protein interactions to form the heterodimer of gp120/41, (2) gp41 interaction sites which form homooligomers of these gp120/41 heterodimers on the virion surface, (3) the T21-like domain of gp41 forming a coiled coil in the fusogenic state only, and (4) the hydrophobic fusogenic peptide at the N-terminus shielded in the native state. The distinction between the two models is in which state the T20−T21 interaction takes place. In model A, the gp41 native state includes antiparallel interactions between monomers corresponding to the T20- and T21-like regions. In model B, it is the fusogenic state of gp41 in which a parallel interaction between the T20 region and a tetrameric T21 domain exists.

Our results demonstrating that the T20−T21 structural interaction requires a tetrameric T21 support the proposal of Matthews et al. which suggested that the T20 sequence interacts with the T21 sequence during the fusogenic state of gp41 (model B). It is in this state that the leucine zipper motif present in T21 forms its tetrameric coiled-coil structure with corresponding T21 sequences on the adjoining gp41 proteins. These data do not support the model of a T20−T21 interaction between two monomers in the native state (model A). We note, however, that the parallel orientation of the T20- and T21-like domains in model B are not supported by the results of Lu et al. which demonstrate an antiparallel orientation (Lu et al., 1995), although other models of membrane fusion can be described which account for these observations as well (Eric Hunter, personal communication).

It has also been proposed that the role of the T20 domain in gp41 may be to control the availability of the T21 domain during the fusion event (Matthews et al., 1994). The presence of T20 tetramers at concentrations greater than 20 μM as shown here suggests that this association could be present in the native state of gp41. Taking into account that 100 spikes composed of gp41 oligomers are present on the surface of the virion (Gelderblom et al., 1987), a tetrameric gp41-oligomerization state (Pinter et al., 1989), and a 50-nm virion radius (Wong-Staal, 1990), it is possible to calculate a concentration of gp120/41 heterodimers per virus particle equal to 1300 μM. Since these heterodimers are confined to the surface of the virion, this corresponds to a lower limit surface concentration of gp120/41 heterodimers. This is well above the 20 μM concentration where T20 tetramers were observed in this experiment. If T20 serves such a role, model B requires that the tetrameric structure spanned by T20 be easily displaced by the coiled-coil structure of the T21 domain. As previously mentioned, experiments have suggested that the T20 self-association is not a tight association and could therefore be easily displaced during a fusogenic transition such as that in model B.

In conclusion, we have used a variety of techniques to characterize two peptides with sequences taken from the transmembrane protein gp41 which have shown potent antiviral activity against HIV-1 in fusion assays. The T21 peptide self-associates in a monomer/dimer/tetramer equilibrium, with a significant concentration of tetramers appearing at 10 μM. The T20 peptide is monomeric at low concentrations and establishes a slowly equilibrating monomer/tetramer self-association at concentrations greater than or equal to 20 μM. These peptides demonstrate a structural interaction at concentrations where T21 is present in the tetrameric form. Examination of truncations and mutations of the T20 sequence has probed the relation of peptide length

and primary sequence to the observed structural interaction and antiviral activity of the peptide. The structural interaction observed is indicative of a binding event between T20 and the tetrameric structure of T21; yet binding is not the sole requirement for antiviral activity. These results provide important clues as to the mechanism of action of each peptide in the inhibition of membrane fusion and to the mechanism of the membrane fusion event itself.

ACKNOWLEDGMENT

HIV-1 $_{LAI}$, CEM, and Molt-4 cells were kindly provided by Dr. T. Matthews of the Duke University Medical Center. The authors thank Michelle Brown, Diana Davis, Bryan Fine, Robyn Medinas, and John Stellwagen for their technical support, Mohammed Anwer, Dennis Lambert, and Michael Recny for their contributions, and Tom Matthews for critical reading of the manuscript.

REFERENCES

Bullough, P. A., Hughson, F. M., Skehel, J. J., & Wiley, D. C. (1994) *Nature 371*, 37−43.

Bustamante, C., Tinoco, I., Jr., & Maestre, M. F. (1983) *Proc. Natl. Acad. Sci. U.S.A. 80*, 3568−3572.

Cao, J., Bergeron, L., Helseth, E., Thali, M., Repke, H., & Sodroski, J. (1993) *J. Virol. 67*, 2747−2755.

Carr, C. M., & Kim, P. S. (1993) *Cell 73*, 823−832.

Chen, C.-H., Matthews, T. J., McDanal, C. B., Bolognesi, D. P., & Greenberg, M. L. (1995) *J. Virol. 69*, 3771−3777.

Chen, S. S.-L., Lee, C.-N., Lee, W.-R., McIntosh, K., & Lee, T.-H. (1993) *J. Virol. 67*, 3615−3619.

Cohen, C., & Parry, D. A. D. (1986) *Trends Biochem. Sci. 11*, 245−248.

Dalgleish, A., Beverly, P., Clapham, P., et al. (1984) *Nature 312*, 763−766.

Dubay, J. W., Roberts, S. J., Brody, B., & Hunter, E. (1992) *J. Virol. 66*, 4748−4756.

Earl, P. L., Doms, R. W., & Moss, B. (1990) *Proc. Natl. Acad. Sci. U.S.A. 87*, 648−652.

Edelhoch, H. (1967) *Biochemistry 6*, 1948−1954.

Fields, G. B., & Noble, R. L. (1990) *Int. J. Peptide Protein Res. 35*, 161−214.

Gallaher, W. R., Ball, J. M., Garry, R. F., Griffin, M. C., & Montelaro, R. C. (1989) *AIDS Res. Hum. Retroviruses 5*, 431−440.

Gelderblom, H. R., Hausmann, E. H. S., Ozel, M., Pauli, G., & Koch, M. A. (1987) *Virology 156*, 171−176.

Hart, T. K., Kirsh, R., Ellens, H., Sweet, R. W., Lambert, D. M., Petteway, S. R., Jr., Leary, J., & Bugelski, P. J. (1991) *Proc. Natl. Acad. Sci. U.S.A. 88*, 2189−2193.

Holzwarth, G., & Doty, P. (1965) *J. Am. Chem. Soc. 87*, 218−228.

Johnson, M. L., & Straume, M. (1994) in *Modern Analytical Ultracentrifugation* (Schuster, T. M., & Laue, T. M., Eds.) pp 37−65, Birkhauser, Boston.

Johnson, M. L., Correia, J. J., Yphantis, D. A., & Halvorson, H. R. (1981) *Biophys. J. 36*, 575-588.

Johnson, W. C., Jr. (1990) *Proteins: Struct., Funct., Genet. 7*, 205−214.

Karber, G. (1931) *Arch. Exp. Pathol. Pharmakol. 162*, 480−483.

Kim, P. S., & Baldwin, R. L. (1990) *Annu. Rev. Biochem. 59*, 631−660.

King, D. S., Fields, C. G., & Fields, G. B. (1990) *Int. J. Peptide Protein Res. 36*, 255−266.

Kippen, A. D., Sancho, J., & Fersht, A. R. (1994) *Biochemistry 33*, 3778−3786.

Kirsh, R., Hart, T. K., Ellens, H., Miller, J., Petteway, S. R., Jr., Lambert, D. M., Leary, J., & Bugelski, P. J. (1990) *AIDS Res. Hum. Retroviruses 6*, 1209−1212.

Lambert, D. M., Barney, S., Lambert, A. L., Guthrie, K., Medinas, R., Davis-Rhodes, D. E., Bucy, T., Erickson, J., Merutka, G., Matthews, T. J., & Petteway, S. R., Jr. (1996) *Proc. Natl. Acad. Sci. U.S.A. 93*, 2186−2191.

Laue, T. M. (1992) *Technical Information DS-835*, Spinco Business Unit, Palo Alto, CA.

Laue, T. M., Shah, B. D., Ridgeway, T. M., & Pelletier, S. L. (1992) in *Analytical Ultracentrifugation in Biochemistry and Polymer Science* (Harding, S. E., Rowe, A. J., & Horton, J. C., Eds.) pp 90−125, Royal Society of Chemistry, Cambridge.

Lu, M., Blacklow, S. C., & Kim, P. S. (1995) *Nature, Struct. Biol. 2*, 1075−1082.

Lumb, K. J., Carr, C. M., & Kim, P. S. (1994) *Biochemistry 33*, 7361−7367.

Manning, M. C. (1989) *J. Pharm. Biomed. Anal. 7*, 1103−1119.

Matthews, T. J., Langlois, A. J., Robey, W. G., Chang, N. T., Gallo, R. C., Fischinger, P. J., & Bolognesi, D. P. (1987) *Proc. Natl. Acad. Sci. U.S.A. 83*, 9709−9713.

Matthews, T. J., Wild, C., Chen, C.-h., Bolognesi, D. P., & Greenberg, M. L. (1994) *Immun. Rev.*, 93−104.

McRorie, D. K., & Voelker, P. J. (1993) *Self-Associating Systems in the Analytical Ultracentrifuge*, Beckman Instruments, Palo Alto, CA.

Milhalyi, E. (1968) *J. Chem. Eng. Data 13*, 179−182.

Monera, O. D., Zhou, N. E., Kay, C. M., & Hodges, R. S. (1993) *J. Biol. Chem. 268*, 19218−19227.

Neurath, A. R., Lin, K., Strick, N., & Jiang, S. (1995) *AIDS Res. Hum. Retroviruses 11*, 189-190.

O'Shea, E. K., Klemm, J. D., Kim, P. S., & Alber, T. (1991) *Science 254*, 539−544.

Owens, R. J., & Compans, R. W. (1990) *Virology 179*, 827−833.

Perczel, A., Park, K., & Fasman, G. D. (1992) *Anal. Biochem. 203*, 83−93.

Pinter, A., Honnen, W. J., Tilley, S. A., Bona, C., Zaghouani, H., Gorny, M. K., & Zolla-Pazner, S. (1989) *J. Virol. 63*, 2674−2679.

Poumbourios, P., McPhee, D. A., & Kemp, B. E. (1992) *AIDS Res. Hum. Retroviruses 8*, 2055−2062.

Poumbourios, P., Ahmar, W. E., McPhee, D. A., & Kemp, B. E. (1995) *J. Virol. 69*, 1209−1218.

Rabenstein, M., & Shin, Y.-K. (1995) *Biochemistry 34*, 13390−13397.

Sattentau, Q. J., & Moore, J. P. (1991) *J. Exp. Med. 174*, 407−415.

Schawaller, M., Smith, G. E., Skehel, J. J., & Wiley, D. C. (1989) *Virology 172*, 367−369.

Shoemaker, K. R., Kim, P. S., York, E. J., Stewart, J. M., & Baldwin, R. L. (1987) *Nature 326*, 563−567.

Shugars, D. C., Wild, C. T., Greenwell, T. K., & Matthew, T. J. (1996) *J. Virol. 70*, 2982−2991.

Tasayco, M. L., & Carey, J. (1992) *Science 255*, 594−597.

Thomas, D. J., Wall, J. S., Hainfeld, J. F., Kaczorek, M., Booy, F. P., Trus, B. L., Eiserling, F. A., & Steven, A. C. (1991) *J. Virol. 65*, 3797−3803.

Wild, C., Oas, T., McDanal, C., Bolognesi, D., & Matthews, T. (1992) *Proc. Natl. Acad. Sci. U.S.A. 89*, 10537−10541.

Wild, C., Greenwell, T., & Matthews, T. (1993) *AIDS Res. Hum. Retroviruses 9*, 1051−1053.

Wild, C., Dubay, J. W., Greenwell, T., Baird, J., Teaster, Oas, T. G., McDanal, C., Hunter, E., & Matthews, T. (1994a) *Proc. Natl. Acad. Sci. U.S.A. 91*, 12676−12680.

Wild, C. T., Shugars, D. C., Greenwell, T. K., McDanal, C. B., & Matthews, T. J. (1994b) *Proc. Natl. Acad. Sci. U.S.A. 91*, 9770−9774.

Wild, C., Greenwell, T., Shugars, D., Rimsky-Clarke, L., & Matthews, T. (1995) *AIDS Res. Hum. Retroviruses 11*, 323−325.

Wiley, D. C., & Skehel, J. J. (1990) in *Virology* (Fields, B. N., Knipe, D. M., Chanock, R. M., Melnick, J. L., Hirsch, M. S., Monath, T. P., & Roizman, B., Eds.) pp 630−685, Raven Press, New York.

Wilson, I. A., Skehel, J. J., & Wiley, D. C. (1981) *Nature 289*, 366−373.

Wong-Staal, F. (1990) in *Virology* (Fields, B. N., Knipe, D. M., Chanock, R. M., Melnick, J. L., Hirsch, M. S., Monath, T. P., & Roizman, B., Eds.) pp 1529−1543, Raven Press, New York.

Yphantis, D. A., Correia, J. J., Johnson, M. L., & Wu, G.-M. (1978) in *Physical Aspects of Protein Interactions* (Catsimpoolas, N., Ed.) pp 275−303, Elsevier/North-Holland, New York.

BI9606962